Journal of Computational Neuroscience (2019) 47:17–30
https://doi.org/10.1007/s10827-019-00719-3

How to correctly quantify neuronal phase-response curves from noisy recordings

Janina Hesse[1,2] · **Susanne Schreiber**[1,2]

Received: 14 January 2019 / Revised: 9 April 2019 / Accepted: 7 May 2019 / Published online: 24 June 2019

Abstract

At the level of individual neurons, various coding properties can be inferred from the input-output relationship of a cell. For small inputs, this relation is captured by the phase-response curve (PRC), which measures the effect of a small perturbation on the timing of the subsequent spike. Experimentally, however, an accurate experimental estimation of PRCs is challenging. Despite elaborate measurement efforts, experimental PRC estimates often cannot be related to those from modeling studies. In particular, experimental PRCs rarely resemble the characteristic theoretical PRC expected close to spike initiation, which is indicative of the underlying spike-onset bifurcation. Here, we show for conductance-based model neurons that the correspondence between theoretical and measured phase-response curve is lost when the stimuli used for the estimation are too large. In this case, the derived phase-response curve is distorted beyond recognition and takes on a generic shape that reflects the measurement protocol and masks the spike-onset bifurcation. We discuss how to identify appropriate stimulus strengths for perturbation and noise-stimulation methods, which permit to estimate PRCs that reliably reflect the spike-onset bifurcation – a task that is particularly difficult if a lower bound for the stimulus amplitude is dictated by prominent intrinsic neuronal noise.

Keywords Phase response curve measurement · Finite phase response curve · Spike onset bifurcation · Intrinsic noise

1 Introduction

Neuronal dynamics are commonly studied based on the response of a neuron to specific stimuli. The spiking in response to post-synaptic currents or temporally structured inputs, for example, often serves as a first indication for the neuronal code. Constraining the response to weak stimuli, a neuron's spiking dynamics can be captured by the so-called *phase-response curve* (PRC) (Ermentrout 1996; Brown et al. 2004; Gutkin et al. 2005). The PRC relates the timing of a short stimulus pulse to the consequential advance or delay of the next spike. PRCs are valuable to decipher single-cell dynamics, such as the neuronal response to a particular input shape, e.g., synaptic inputs (Reyes and Fetz 1993a; Netoff et al. 2005) or noise (Ermentrout et al. 2008), as well as the locking time to a time-dependent stimulus (Kuramoto 1984; Achuthan et al. 2011). Beyond single cells, PRCs are used to predict how neurons behave when weakly connected, informing about network dynamics and, in particular, their synchronization state (Van Vreeswijk et al. 1994; Hansel et al. 1995; Ermentrout 1996; Galán et al. 2005; Teramae and Fukai 2008; Smeal et al. 2010). Beyond the neurosciences, the PRC is used for various other biological oscillations such as cardiac pacemakers or circadian rhythms (Guevara et al. 1981; Minors et al. 1991).

In order to estimate PRCs experimentally, neuronal spiking is perturbed by a stimulus known by the experimenter (Schultheiss et al. 2011). While the stimulus amplitude might be dictated by the experimental setting, the theoretical PRC is defined in the limit of small stimulus amplitudes and is thus also called the *infinitesimal PRC* (iPRC). We here test under which conditions experimentally measured PRCs actually reflect the theoretical iPRC. Only the latter allows one to draw conclusions about the behavior of

Action Editor: Nicolas Brunel

✉ Janina Hesse
janina.hesse@bccn-berlin.de

[1] Institute for Theoretical Biology, Humboldt-Universität zu Berlin, Philippstr. 13, 10115 Berlin, Germany

[2] Bernstein Center for Computational Neuroscience Berlin, Philippstr. 13, 10115 Berlin, Germany

weakly driven or weakly coupled oscillators, or about the spike-onset bifurcation (Ermentrout 1996, 2010).

Spiking in neurons can be classified into distinct mechanisms of spike initiation, which influence neuronal coding (Izhikevich 2007; Brown et al. 2004; Schleimer and Stemmler 2009; Blankenburg et al. 2015; Hesse et al. 2017). Close to spike onset, the underlying bifurcations are associated with generic iPRCs (Ermentrout 1996; Izhikevich 2000; Schleimer and Schreiber 2018). In order to deduce information about the spike-onset dynamics from measured PRCs, we focus on mean-driven neurons with low firing rates (Schreiber et al. 2009). Summing up, PRCs reflecting the iPRC, which allow us to derive a multitude of coding properties for individual cells as well as neuronal populations, require an experimental setup with low firing rates and small stimulus amplitudes.

The experimental choice of the appropriate stimulus size is a non-trivial problem (Netoff et al. 2011). As we show in the following, the measurement of a PRC that reflects the iPRC requires a stimulus amplitude from a range bounded from below and from above: On one hand, the experimental stimulus has to be chosen large enough to overcome intrinsic noise, which perturbs spiking in addition to the stimulus (Manwani and Koch 1999). On the other hand, the stimulus has to be weak enough such that the PRC fulfills the required theoretical assumptions: Stimulus amplitudes have to be sufficiently small to allow the dynamics to relax back to the limit cycle within one period, because the PRC, as a linear approximation of the dynamics, assumes independence of subsequent spikes (Ermentrout and Terman 2010). As a rule of thumb, the larger the intrinsic noise, the more restricted the range of acceptable stimulation amplitudes.

Relatively strong intrinsic noise is, for example, typical for cortical and hippocampal neurons, which can show notable spike jitter even for constant step current stimuli (Mainen and Sejnowski 1995; Fellous et al. 2001; White et al. 1998; Diba et al. 2004). We show that the consequential variability of the phase response observed experimentally can impair PRC measurements (Wang et al. 2013; Stiefel and Ermentrout 2016). This was not observed previously because the methods for quantification of PRCs were typically illustrated with neurons showing only low levels of intrinsic noise, and thus stable firing rates; for a review see Torben-Nielsen et al. (2010a).

In the following, we compare the measurement accuracy of three different PRC methods faced with strong intrinsic noise. While Torben-Nielsen et al. (2010a) have previously considered different methods under relatively benign conditions, we are interested in extreme conditions with large stimuli or large intrinsic noise levels. Exploring the border where a PRC estimation can no longer be related to the theoretical iPRC allows us to delineate the range of experimental conditions under which PRC measurements can be expected to actually yield information on the linearized neuronal dynamics.

2 Methods

2.1 Models

PRCs were measured for conductance-based neuron models with three different spike onset bifurcations, for details see Appendix. Of the possible limit cycle bifurcations for spike initiation (Izhikevich 2007), we have chosen those that result in biologically realistic all-or-none spikes with finite voltage amplitude at spike onset: the *subcritical Hopf* bifurcation, the *saddle-node on invariant cycle* (SNIC) bifurcation and the *saddle-homoclinic orbit* (HOM) bifurcation. The level of the intrinsic noise was set by the standard deviation of an additive zero-mean white-noise current, see Appendix.

2.2 Phase-response curve

For a regular spiking conductance-based neuron model with baseline period T (firing rate $f = 1/T$), weakly perturbed spiking can be described by an input-output equivalent phase oscillator (Lazar 2007),

$$\dot{\varphi} = 1 + Z(t)s(t), \tag{1}$$

with Z as PRC, and a time-dependent stimulus $s(t)$. We enumerate the temporally ordered spike times with an index i, i.e., spikes occur at times $t = \{t_i\}$. In response to the stimulus $s(t)$, the spike at $t = t_{i+1}$ following the spike at $t = t_i$ is advanced or delayed according to the phase deviation (Kuramoto 1984),

$$\Delta\varphi = \int_{t=t_i}^{t_i+T} Z(t)s(t)\mathrm{d}t, \tag{2}$$

i.e., the effect of the input on the subsequent spike is integrated over the inter-spike interval.

2.3 Theoretical estimation of the iPRC

The theoretical iPRC can be defined as the derivative of the phase with respect to the input, i.e., it assumes infinitesimally small inputs, hence the name infinitesimal phase-response curve. Because the iPRC captures the linearized dynamics of the neuron, it describes the response of a neuron to small inputs, i.e., inputs that are small enough to ignore non-linear effects. The iPRC captures to first order changes in the timing of the limit cycle, while neglecting changes to the limit cycle amplitude.

For mathematical neuron models, the iPRC can be gained by numerical integration, for a review see Govaerts and Sautois (2006): For a conductance-based neuron model with equation $\dot{x} = F(x)$, the linearized dynamics on the limit cycle are given as $\dot{x} = Jx$ with the Jacobian $J = \frac{\partial F}{\partial x}$. The corresponding adjoint equation is $\dot{y} = -J^{\mathrm{T}} y$. As the adjoint dynamics are unstable, backward integration in time along the limit cycle leads to a stable solution y, whose first entry corresponds to the voltage PRC (Ermentrout and Kopell 1991, 1996). We use this method to derive the theoretical, infinitesimal PRC for the models. The comparison of theoretical iPRC and PRCs estimated with experimentally-inspired methods allows us to suggest the appropriate input strength, as well as a reasonable noise level, both of which can be employed in biological experiments to prevent PRC measures as mentioned in the introduction, which are less informative about neuronal dynamics compared to PRC estimates that can be related to the theoretical iPRC.

2.4 Experimental methods of PRC measurements

We consider three different methods for PRC estimation (Torben-Nielsen et al. 2010a; Schultheiss et al. 2011). The estimation analyzes spike timing in response to a known stimulus. For the first method, neuronal spiking is perturbed by a sequence of short current pulses, the other two methods use a noise stimulus. In addition, the neuron is stimulated with a DC current that ensures repetitive spiking; we choose a baseline firing rate of 10Hz (i.e., with period T = 100 ms). The simulation duration is sufficient to record about 500 perturbed spikes, for details see Appendix. Programming code for numerical simulations, data analysis and figure plotting are available from zenodo.org, doi: 10.5281/zenodo.2628349.

For two consecutive spikes at time $t = t_i$ and $t = t_{i+1}$, the actual interspike interval duration is $\mathrm{ISI}_i = t_{i+1} - t_i$. For the phase response, we normalize the time during the unperturbed period T to a phase variable φ that ranges from zero to one. For a perturbed interspike interval, the change in duration is captured by the *phase deviation*, $\Delta\varphi_i = 1 - (t_{i+1} - t_i)/T$, which is positive for spike advances, and negative for phase delays. For PRCs that reflect the theoretical iPRC, the amplitude of the phase deviation $\Delta\varphi$ scales linearly with the stimulus strength. The amplitude of the PRC in response to a current stimulation is recovered by dividing the phase deviation by the temporal integral over the input stimulus during one interspike interval. This integral corresponds to the product of the appropriate input strength and the temporal resolution of the measured PRC, as detailed below. The resulting PRC has units of phase per current per time (for conductance-based models implementing a current per surface area this results in Hz $\mathrm{cm}^2/\mu\mathrm{A}$). Here, we use the PRC unit 1/mV that directly allows for a comparison with the theoretical iPRC, for details on the conversion see Appendix.

For plotting purposes, PRCs are commonly fitted either with polynomial functions, e.g., Netoff et al. (2005), or with Fourier series consisting of a low number of Fourier coefficient, e.g., Galán et al. (2005). Because the theoretical iPRC is by construction a periodic function, we here use Fourier series that enforce per definition periodic boundary conditions. As we are also interested in PRCs with steep components (such as the PRC of the HOM model in Fig. 2a), we fit our PRC estimates with a Fourier series of order five (i.e., with 11 Fourier components) that grants sufficiently high frequencies,

$$Z(\varphi) = a_0 + \sum_{j=1}^{5} \left(a_j \cos(2\pi j\varphi) + b_j \sin(2\pi j\varphi)\right), \qquad (3)$$

with Fourier coefficients $a_0, a_1, ...a_5, b_1, ..., b_5$. Using the same number of Fourier components for all PRC estimates facilitates the comparison of different methods.

2.4.1 PRC estimation based on individual-timepoint perturbation

For the PRC estimation based on individual-timepoint perturbations (Reyes and Fetz 1993b; Galán et al. 2005; Tsubo et al. 2007), the repetitively spiking neuron is stimulated with short delta-like current pulses of a specific amplitude α, for specific values see Table 2 in the Appendix. The perturbation method was chosen for most experimentally measured PRCs reported in the literature (Reyes and Fetz 1993a, b; Goldberg et al. 2007; Tsubo et al. 2007; Wang et al. 2013), as it is intuitive and easily analyzed.

The analysis evaluates interspike intervals in which a current pulse occurs. Here, the interval between two successive pulses is chosen randomly between 150 ms and 250 ms, such that most perturbations occur as single events in every second interspike interval. This ensures the independence of subsequent perturbations, allowing the dynamics a whole period to relax. The timing of the perturbation is related to the resulting phase deviation, compare Fig. 1a. Given a current pulse at $t = t_p$ between two consecutive spikes at $t = t_i$ and $t = t_{i+1}$, the PRC relates the phase deviation, $\Delta\varphi_i = 1 - (t_{i+1} - t_i)/T$, to the phase at which the current pulse occurred, $\varphi_i^p = (t_p - t_i)/T$ (Rinzel and Ermentrout 1989). An estimate of the PRC in units of phase deviation is gained by plotting the phase deviation against the perturbation phase. More precisely, each point of this graph corresponds to a stochastic drawing from the underlying PRC. In order to get the PRC in response to current perturbations, the PRC in units of phase deviation is divided by the amplitude of the perturbation

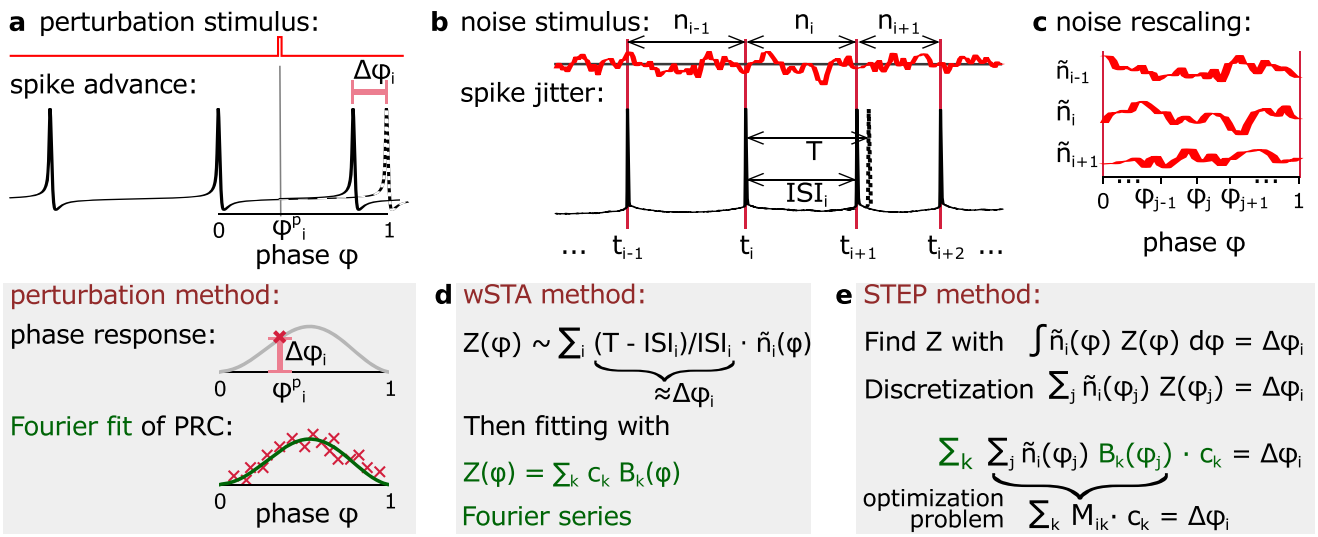

Fig. 1 Experimental methods for PRC measurements and curve fitting with a Fourier series (fitted PRC $Z(\varphi) = \sum_k c_k B_k(\varphi)$ with Fourier components c_k and base functions $B_k(\varphi)$). **a**: Individual time-point perturbation. The phase deviation $\Delta\varphi$, resulting from stimulation with a short current pulse, is plotted against the timing of the current pulse, and fitted by a curve. **b**: Time-continuous noise stimulation. Spike times t_i are jittered due to a continuous noise stimulation, resulting in interspike intervals ISI_i around the baseline period T. **c**: The noise injected during one interspike interval $n_i(t)$ is mapped to the phase variable by rescaling the interspike interval to the range from zero phase to phase one, resulting in the shown noise snippet $\tilde{n}_i(\varphi)$. The discretization of the phase in uniformly distributed values φ_j is used by the STEP method (see e). **d**: The wSTA method estimates the PRC via a weighted spike-triggered average. The PRC is proportional to the sum over the noise snippets $\tilde{n}_i(\varphi)$ (this resembles a spike-triggered average), weighted by the phase deviation with respect to the current interspike interval, $\Delta\varphi_i \approx (T - \mathrm{ISI}_i)/\mathrm{ISI}_i$. **e**: The STEP method relies on an error minimization of the input-and-PRC-based prediction of spike jitter. The phase deviation $\Delta\varphi_i$ induced by the noise snippet n_i is predicted by a temporal integral over the product of noise stimulus and PRC. Replacing the integral by a sum over the discretized phases φ_j, and the PRC by its Fourier series, results in a double sum, which allows for the identification of an optimization matrix M (with rows M_k). With this, the STEP method interprets the prediction of the phase deviation as an optimization problem for the PRC Fourier components c_k

stimulus and the duration of the current pulse, $Z(\varphi) = \Delta\varphi(\varphi)/(\alpha\tilde{\tau})$, where $\tilde{\tau}$ corresponds for the perturbation methods to the duration of an individual perturbation (in our case $\tilde{\tau} = 0.1$ ms).

For neurons with intrinsic noise, even weak noise perturbs the raw data so strongly that the PRC shape can often not be identified by naked eye. To fit a curve to the raw PRC data, we here use Galán's method (Galán et al. 2005; Netoff et al. 2011), for which the Fourier components of Eq. (3) are given for a set of N perturbed spikes as

$$a_0 = \frac{1}{N}\sum_{i=1}^{N}\Delta\varphi_i, \quad a_j = \frac{1}{N}\sum_{i=1}^{N}\Delta\varphi_i \cos(2\pi j\varphi_i^p),$$
$$b_j = \frac{1}{N}\sum_{i=1}^{N}\Delta\varphi_i \sin(2\pi j\varphi_i^p).$$

2.4.2 PRC estimation based on time-continuous noise stimulation

For the PRC estimation based on noise-stimulation, the repetitively spiking neuron is stimulated with a zero-mean noise stimulus (Izhikevich 2007). We use a colored noise current with time resolution of dt=0.01 ms with standard deviation γ (for specific values see Table 2 in the Appendix), resulting from filtering a white noise signal with a cut-off frequency of 1000 Hz.

For each spike, the recorded phase deviation $\Delta\varphi_i$ is related to the noise snippet n_i that corresponds to the preceding interspike interval, see Fig. 1b. The duration of the noise snippet $n_i(t)$ is rescaled to the phase variable, resulting in a phase-dependent noise snippet $\tilde{n}_i(\varphi)$, see Fig. 1c.

To estimate PRCs from the noise-stimulated spike trains, we use the *weighted Spike-Triggered Average* (wSTA) introduced by Ota et al. (2009) and the *STandardized Error Prediction* (STEP) method introduced by Torben-Nielsen et al. (2010b).

The wSTA method sums over the phase-dependent noise snippets, while weighting each noise snippet by a variant of the phase deviation, $\bar{\Delta\varphi} = T/(t_{i+1} - t_i) - 1$, see Fig. 1d (Ota et al. 2009). For the correct amplitude scaling, the result is then divided by the variance of the noise input, γ^2.

The STEP method optimizes the PRC shape to predict the phase deviation caused by the noise input since the previous spike (Torben-Nielsen et al. 2010b). The idea takes advantage of Eq. (2), which predicts the phase deviation resulting from the stimulus $s(t) = n_i(t)$. Both the PRC

and the phase-dependent noise snippets are discretized by a temporal binning with 200 phase bins. This allows one to replace the integration in Eq. (2) by a simple sum of the PRC and the phase-dependent snippet $\tilde{n}_i$ (Fig. 1e). To create an optimization matrix M, the binned versions of noise and base functions are multiplied (Fig. 1e). Linear least square optimization (here we used the python function `numpy.linalg.lstsq()`) permits finding the Fourier coefficients that, when multiplied by the matrix M, best recover the phase deviations extracted from the raw data of spike times.

In order to get the PRC in response to current perturbations, the PRC in units of phase deviation is divided by the standard deviation of the noise stimulus, $Z(\varphi) = \Delta\varphi(\varphi)/(\gamma\tilde{\tau})$, where $\tilde{\tau}$ corresponds for the noise-stimulation method to the time bin used to evaluate the PRC (i.e., spiking period divided by the number of data points per PRC estimate, in our case $\tilde{\tau} = T/200$).

An advantage of the perturbation method and the wSTA method compared to the STEP method is that the PRC estimates can be implemented as an ongoing process that continuously allows one to add new data as it becomes available. In contrast, the STEP method, and similar methods that rely on spike prediction error minimization, require a set of noise/spike-timing pairs of a fixed size, and, at least in current implementations, the optimization has to be redone when new data is collected.

3 Results

In order to measure PRCs experimentally from repetitively firing neurons, the spike times are perturbed by an additional stimulus consisting of either a noise current or short pulse-like perturbations. Under the assumption that the stimulus has to be weak, intrinsic noise in real neurons makes the appropriate scaling of the stimulus amplitude a non-trivial problem (Netoff et al. 2011). The stimulus has to be large enough to stand out against the intrinsic noise, yet also small enough to prevent the instantaneous induction of spikes.

While most previous studies focus on the PRC shape, and neglect the PRC amplitude, we here also evaluate the PRC amplitude. The PRC amplitude is essential for a quantitative comparison of measurements, as it scales quantities derived from the PRC such as the synchronization range or the transition time until locking is established (Kuramoto 1984).

3.1 PRC estimates with perturbations or noise stimuli

Figure 2a-b shows PRC estimates for models without intrinsic noise with three different spike generation mechanisms (top to bottom), using three different methods (left to right: perturbation method, wSTA method and STEP method), see Methods for details. For comparison, each small panel depicts the theoretical iPRC (brown) and PRCs estimated from spiking in response to different stimulus strengths (color-coded from green to violet, see Appendix for specific values). While all three methods estimate the shape of the PRC with similar quality, the STEP method has a tendency to overestimate the amplitude of the PRC, which is not observed for the perturbation method and the wSTA method.

For the Hopf model, the PRC derived with the wSTA method seems reasonable. In contrast, the perturbation method and the STEP method both lead to strongly wiggling PRCs for intermediate stimulus amplitudes, see Fig. 2a and b. The wiggling PRCs occur for stimulus amplitudes for which the model becomes extremely sensitive to inputs (the coefficient of variation shows a maximum in response to these noise strengths). As a side-note, this behavior was also observed for another model with subcritical Hopf bifurcation at spike onset, the original Hodgkin-Huxley model (Hodgkin and Huxley 1952).

3.2 Stimulus amplitude dependence

The range of stimulus amplitudes in Fig. 2a and b is chosen to illustrate the transition of PRC estimates from a regime that reflects the theoretical iPRC, to a regime that mostly reflects the measurement protocol. Because the models lack intrinsic noise, the theoretical curve (brown) is best fitted by the PRC with the lowest input strength (green), and reasonable fits are derived for a range of small stimulus levels. The correspondence between theoretical and estimated PRC is lost for intermediate stimulus levels, and the estimated PRC approaches a stereotypical shape for large stimulus levels. Figure 2c and d summarizes the PRC estimates corresponding to the largest stimulus strength (the violet curves from Fig. 2a and b). In these cases, the estimated PRC deviates in a characteristic way from the iPRC. Because the shape is hardly distinguishable for different spike generation mechanisms, the PRC is not informative about spike onset. Indeed, the measured PRC shape reflects the measurement protocol, but not the underlying spike-onset bifurcation. With such a large input, the drive is too strong to estimate PRCs that reflect the iPRC, and we call this regime in the following the *overdriven* regime.

3.3 Shape of overdriven PRCs

The stereotypical PRC shape in the overdriven regime (Fig. 2c and d) shows a linear relation for intermediate phases, with a steep connection around phase zero that is enforced by the periodicity of the Fourier-series fit.

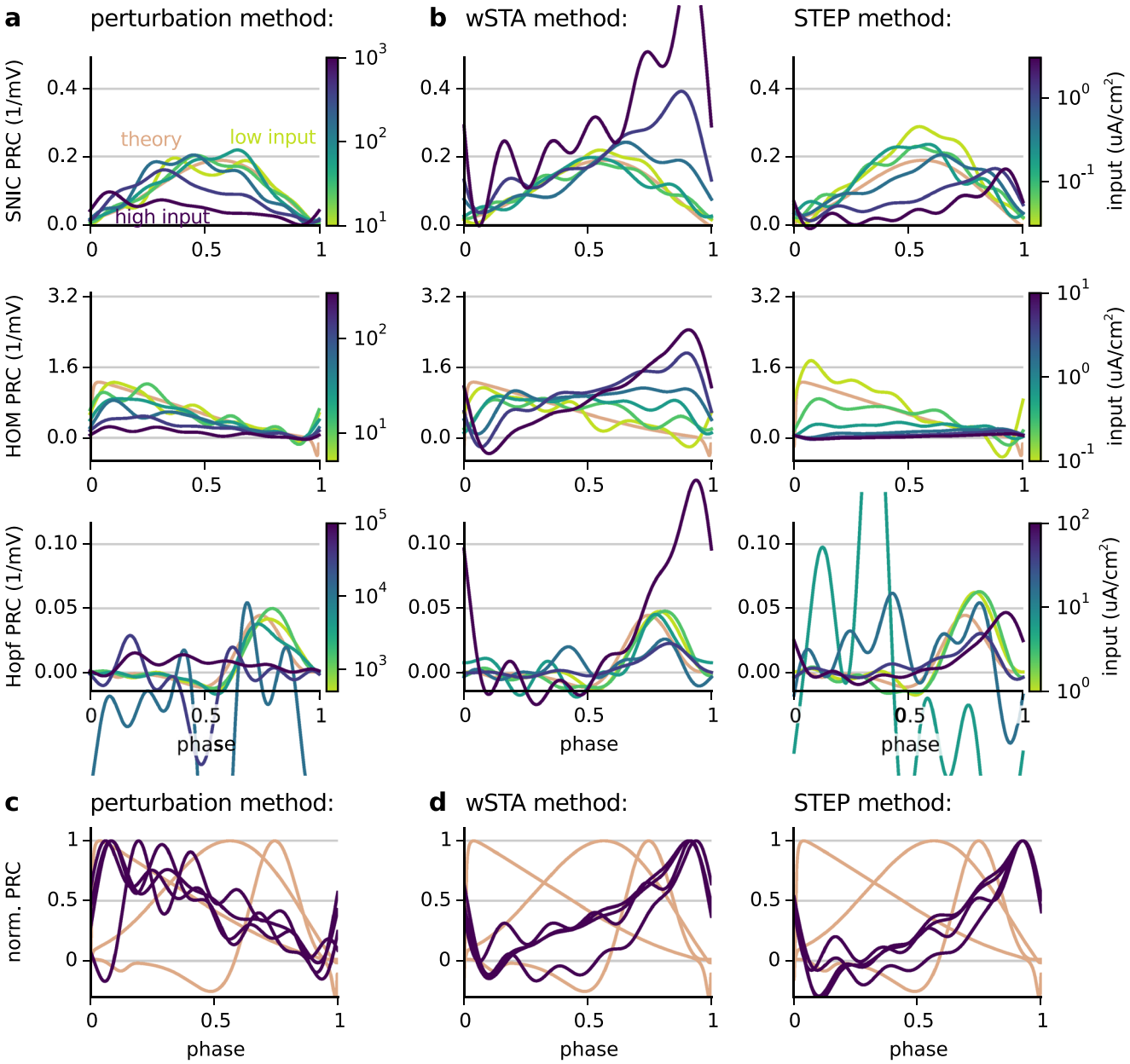

Fig. 2 Comparing PRC measurements for three spike generation mechanism (input strength is color-coded from green to violet). The smooth theoretical iPRC is depicted in brown. **a**: PRCs measured with the perturbation method. **b**: PRCs measured with wSTA and STEP method. **c**-**d**: Comparison of models with different spike-onset bifurcations, PRCs measured with the highest stimulus amplitude from (**a**-**b**). This strongest stimulus leads to a PRC shape that is no longer specific to the neuron models with different spike-onset bifurcations, but only reflects the measurement method (perturbation or noise-stimulation method)

The linear decrease/increase observed for the perturbation and noise-stimulation methods, respectively, results from instantaneous spikes in response to large perturbations in the stimulus.

For the perturbation method (Fig. 2c), the instantaneous initiation of spikes results in larger phase advances for earlier perturbation phases, which directly translate into a linear decrease, see Fig. 3a. For the overdriven PRC in units of phase deviation, the slope of the PRC is minus one, which has been termed the *causality limit* (Netoff et al. 2011) or *causal limit* (Wang et al. 2013).

For the noise-stimulation methods, spikes are mostly induced by spontaneous, large deviations of the noise stimulus. As a result, the noise snippets show an exceptionally large amplitude right before the spike, i.e., close to phase one (Fig. 3b). Adding those snippets up in a weighted spike-triggered average transfers the large amplitude close to phase one to the PRC, which eventually results in a linearly

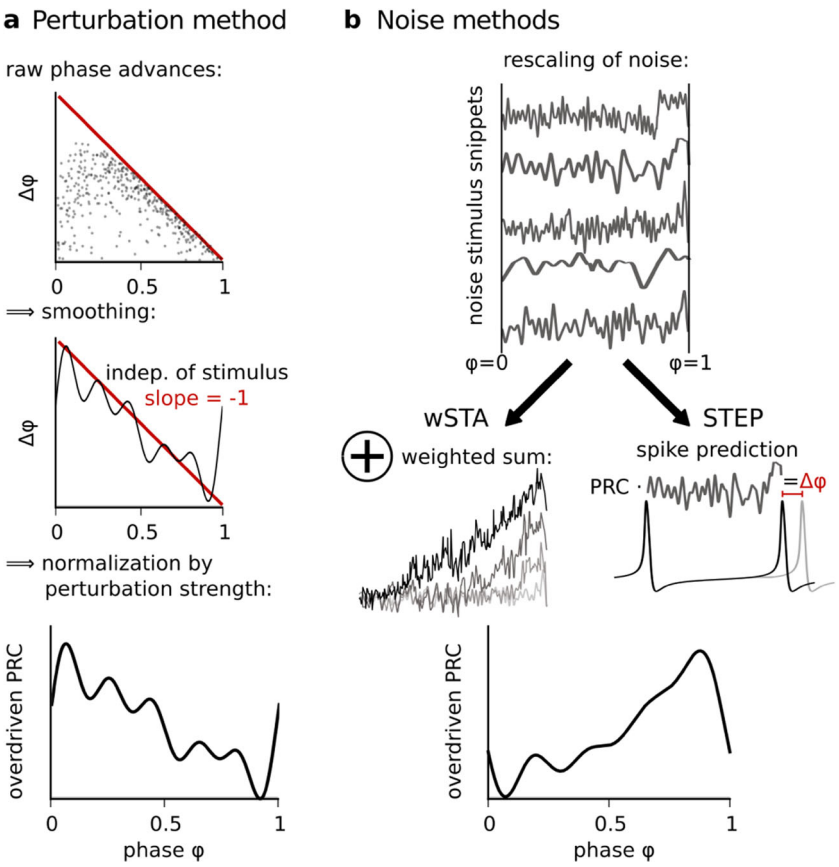

Fig. 3 Perturbation and noise-stimulation methods with large stimulus amplitudes lead to different but stereotypic overdriven PRCs. **a**: For the perturbation method, the overdriven PRC result from the advance of the spike to the time point of the perturbation. **b**: The shape of the overdriven PRC results for the noise stimulation methods from temporally stretched noise snippets with an elevation before the following spike

increasing overdriven PRC (Fig. 2d). Also for the STEP method, this temporal stretching induces a bias. As the neuron seems to react particularly sensitively to inputs right before the spike, it again induces a large PRC amplitude close to a phase equal to one.

How easily an overdriven PRC can be confounded with a real PRC depends on the combination of theoretical iPRC and estimation method. For example, the overdriven PRC of the perturbation method can be easily mistaken for the iPRC of a HOM spike generation, while the overdriven PRCs of the noise-stimulation methods might be mistaken for the iPRC of a Hopf spike generation.

3.4 Dependence on internal noise

When measuring PRCs in biological neurons, recordings will be perturbed by various intrinsic noise sources including ion channel noise and recording noise (Manwani and Koch 1999). We next test the stability of PRC estimates for models implementing intrinsic noise with a strong, yet biologically realistic standard deviation, see Appendix for details.

With intrinsic noise, we observe an intermediate stimulus strength that leads to optimal PRC estimates (third column in Fig. 4). For small stimulus amplitudes, the stimulus' effect on spike timing is veiled by the intrinsic noise, which jitters the spikes more than the stimulus. This results in PRC estimates hardly above noise level, and the quality of the PRC estimates augments with increasing stimulus amplitude (Fig. 4, from the first to the third column), while the estimation error decreases. Further increase in the stimulus amplitude leads to the overdriven regime, first indications of which are visible in the forth column of Fig. 4; the shift in the peak (compare Fig. 2a and b) will continue with increasing stimulus amplitude until the linear PRC is fully established. The error amplitude continues to decrease with stimulus amplitude in the overdriven regime (data not shown). Indeed, the overdriven regime implies a stark, unrealistic reduction in both error types, which shows in published experimental results (Reyes and Fetz 1993a, b; Goldberg et al. 2007).

A comparison between two intrinsic noise levels demonstrates that, as expected, larger intrinsic noise results in larger errors and increases the minimal possible stimulus amplitude (Fig. 4, stronger noise in bottom panels compared to top).

Interestingly, all PRC estimation methods result in a comparable PRC quality (similar shape, amplitude and error levels). This result contrasts previous suggestions that the noise-stimulation method should be less disturbed

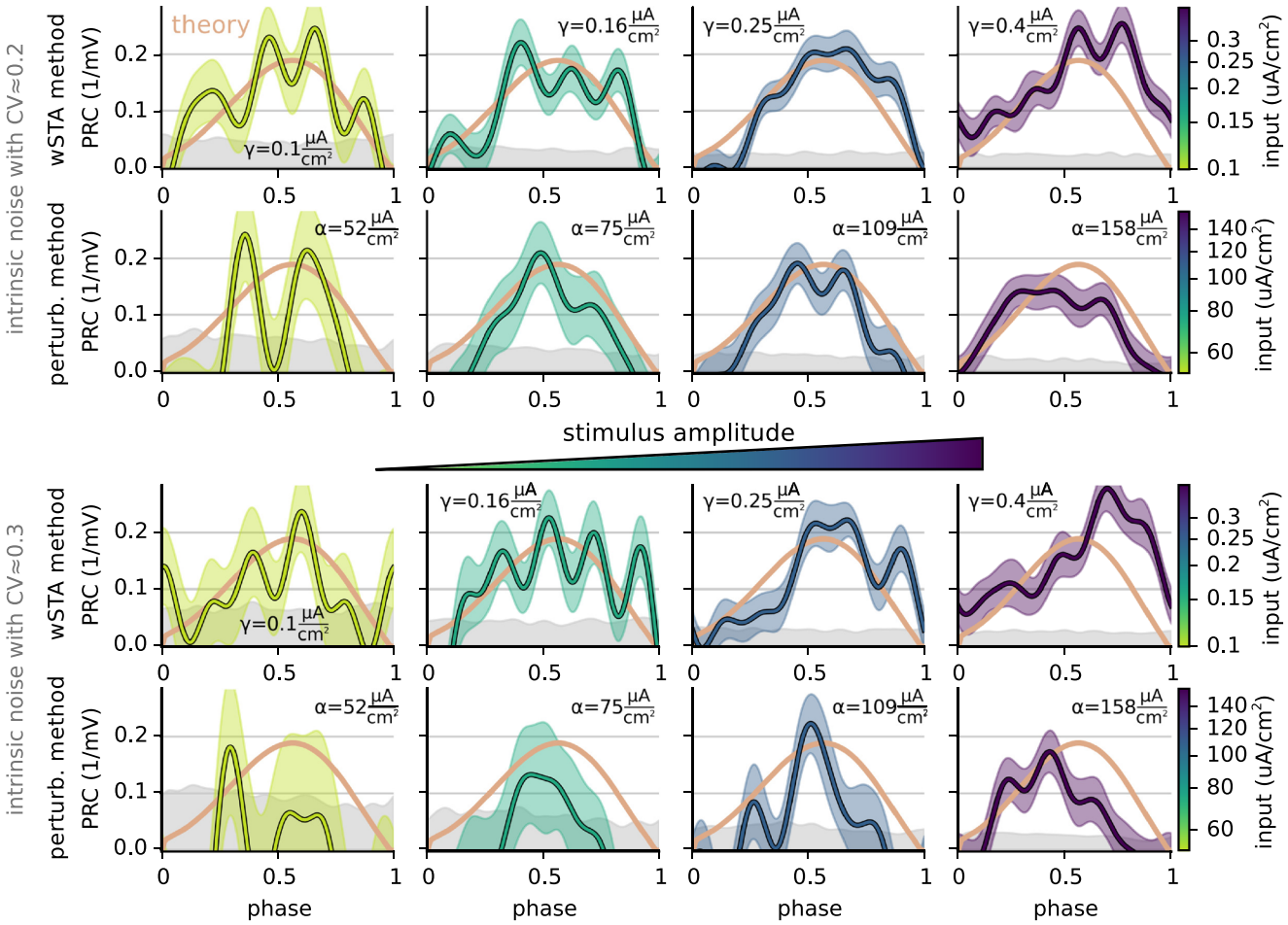

Fig. 4 Perturbation and noise-stimulation methods perform similar under high intrinsic noise levels. The PRC estimation is exemplified with the SNIC model, theoretical iPRC in brown, stimulus strength color-coded and additionally denoted in the panels (noise stimulus standard deviation γ and current pulse amplitude α, respectively); the intrinsic noise is adapted to a baseline coefficient of variation (CV) of 0.2 and 0.3, respectively. For the bottom traces, the PRC estimation directly reaches the overdriven regime once the stimulus amplitude is large enough to counter the intrinsic noise, not allowing for an intermediate, appropriate range of stimulus amplitudes. Bootstrapping of the data results in standard deviation errors for the PRC (transparent colored area) and for the zero-PRC background (gray area), see Appendix

by intrinsic noise compared to the perturbation method (Izhikevich 2007; Netoff et al. 2011). In Fig. 4, even strong intrinsic noise that induces a baseline coefficient of variation (CV) of about 0.2 leads to similar PRC estimates for all methods, while small differences might be observed for slightly higher noise levels with a CV of about 0.3, which is close to the maximum intrinsic noise that still allows one to derive PRCs.

3.5 Practical scaling of the input signal

When measuring PRCs from an experimentally recorded neuron, what is the correct amplitude of the signal? Our results suggest that for neurons with low baseline firing rate around 10 Hz, the stimulus in addition to the DC current (i.e., perturbation or noise) should increase the firing rate by less than 10% above baseline (i.e., when stimulated only with the DC current). The increase in firing rate results from the positive mean value of the PRC observed for most neurons, which predicts that positive inputs will, on average, advance spikes to earlier phases. The stronger the input amplitude, the larger the increase in firing rate. In particular, our data suggests for neurons with low baseline firing rate around 10 Hz, that the overdriven regime correlates with a relative increase in firing rate exceeding 10%. Note that this simple rule of thumb can only be expected to hold close to spike onset, due to the universality induced by the spike onset bifurcation.

So far, common practice recommended to aim for noise stimuli that are sufficiently large to induce voltage deflections on the order of 1 mV, visible by bare eye (Netoff et al. 2011). Yet, experimental results complying with these recommendations already show indications of the overdriven regime (Reyes and Fetz 1993b; Goldberg

et al. 2007). Also in our simulations, we found that at least for neurons with relatively high intrinsic noise, this best practice overestimates the required stimulus amplitude and thus results in overdriven PRCs.

To bound the stimulus amplitude, one could consider the increase in spike jitter due to the stimulation, as measured by the coefficient of variation (CV). In our numerical simulations, the resulting CV can be relatively large (up to a CV of 1) without reaching the overdriven regime, depending on the neuronal dynamics. Accordingly, we found absolute CV values to be of minor help to establish the correct stimulus amplitude.

To summarize, a correct stimulus amplitude is indicated by a relative increase in firing rate by maximally 10% when adding the stimulus to the DC current. In contrast to the common assumption that the perturbing stimulus should be clearly identifiable against the intrinsic noise, the stimulus signal is in this case not visible by eye in the interspike voltage trace.

3.6 Checking the PRC estimate

The reporting of overdriven PRCs is undesirable, because they can severely misrepresent neuronal dynamics when interpreted analog to iPRCs. To check the quality of PRC estimates, we propose three post-experimental analyses.

As mentioned above, one hallmark of the overdriven regime is an unrealistically low level of estimation errors, see Section 3.4. Thus, reported PRCs should always be complemented by meaningful error bars, like those based on bootstrapping (described in the Appendix).

The recording of PRC data for multiple stimulus amplitudes provides a good test against overdriven PRCs for all estimation methods. For the perturbation method, this was previously recommended to identify stimuli that are too weak (Achuthan et al. 2011). We argue that after normalization with the stimulus strength, the amplitude of all PRC estimates with appropriate stimulus strength is comparable, while stimuli with too large an amplitude deviate and show a larger (wSTA) or smaller (STEP and perturbations) PRC amplitude. These size effects are easily singled out in recordings, in contrast to the above described alterations in PRC shape, which could be confused with the unknown, actual iPRC shape as described in Section 3.3. Recording multiple stimulus amplitudes thus helps to spot overdriven PRCs, yet at the cost of a prolongation of the total recording duration.

The noise-stimulation methods provide a clear hallmark of overdriven PRCs without prolongating the recording duration when the same set of recorded spikes is evaluated with the wSTA as well as the STEP method. As can be seen in Fig. 2b, both noise-stimulus methods yield similar PRC amplitudes as long as the input strength is appropriate. Yet, the effect of overdriven stimulation on the PRC amplitude is opposite for both methods. We thus propose to estimate PRCs from the same data via STEP and wSTA methods. A comparison of their respective amplitudes allows one to distinguish between non-overdriven and overdriven PRC measurements: Only if the corresponding PRCs are of similar amplitude and shape, the measurement was performed with an appropriate input strength. If the estimated PRCs differ considerably in their (mean) amplitude, the measurement was most likely overdriven, even if the PRC shape looks similar for both the STEP and the wSTA method. Let's consider two PRCs generated by the STEP and the wSTA method, respectively (denoted $Z_1 \pm \mathrm{SD}_1$ and $Z_2 \pm \mathrm{SD}_2$ with standard deviations $\mathrm{SD}_i, i \in [1, 2]$ as measured by the bootstrapping detailed in the Appendix), using the same resolution in phase for the fitted Fourier series. One approach to evaluate the similarity between both PRCs relies on the difference $\Delta Z = Z_1 - Z_2$, with the associated standard deviation $\mathrm{SD}_\Delta = \sqrt{\mathrm{SD}_1^2 + \mathrm{SD}_2^2}$. Normalizing the difference as $\Delta Z / \mathrm{SD}_\Delta$, its values are expected to be distributed normally around zero with standard deviation one, if the two PRCs are similar. This can be tested by various normality tests, such as the Shapiro-Wilk test or the Anderson-Darling test (Razali and Wah 2011). The here proposed comparison of wSTA and STEP method can also be applied to existing data, as it is based on the same experimental recording being analyzed in two different ways.

4 Discussion

Neuronal phase-response curves have been measured for over twenty years (Reyes and Fetz 1993a, b). PRCs are valuable to analyze neuronal dynamics, and can be used to predict synchronization and locking behavior of the neuron. We report pitfalls of experimental PRC measurements by comparing theoretical iPRCs with PRCs estimated based on simulated spike trains. We find that reliable PRC estimates require an intermediate stimulus amplitude, sufficiently high to overcome intrinsic noise, but not too high to infringe fundamental PRC assumptions. As a result of the analysis, we propose to use stimulus amplitudes that change the low baseline firing rate by not more than 10% and that do not visibly impair the spike train. Stimulus amplitudes that are too large result in overdriven PRCs. Mild cases of overdriven PRCs are marked by a linear increase or decrease with reduced PRC error at low or high phases, respectively. Comparable hallmarks can be observed in previous experimental PRC measurements (Reyes and Fetz 1993a, b; Goldberg et al. 2007; Farries and Wilson 2012a, b; Wang et al. 2013). Even for mildly overdriven PRC estimates, information about neuronal dynamics may be

occluded and conclusions based on these PRCs should be derived with care.

While experimental studies often refer to their estimated PRCs as "finite" PRCs, due to the finite, i.e., non-zero, stimulus amplitude of the experimental set-up, we here show that the distinction between "finite" PRC and the theoretical "infinitesimal" PRC is questioned by our results. We find that PRCs estimated with finite stimulus amplitude either fit the iPRC, or they are less informative about neuronal dynamics: For stimuli that are too small, PRCs estimates are below noise level, and for stimuli that are too large, the PRCs approach a method-specific, generic shape that depicts the neuron misleadingly as a simplistic response machine. In the extreme overdriven regime, the shape of the PRC only reflects the instantaneous generation of a spike in response to a large input, and becomes independent of the neuron type. The transition from PRCs hardly above noise level, to PRCs with clear overdriven characteristics, is also observed in experimental studies with an increase in stimulus amplitude (Reyes and Fetz 1993a; Netoff et al. 2005). As these experimental examples show no clear PRC estimate that lies between intrinsic-noise-dominated and overdriven, the range of appropriate, intermediate stimulus amplitudes seems to be relatively small for the recorded hippocampal and cortical cells.

Here, we have compared PRC estimations for three methods. With optimal stimulus amplitude, all methods perform similarly (Torben-Nielsen et al. 2010a), and, contrary to previous assumptions (Izhikevich 2007; Netoff et al. 2011), we show that even under noisy conditions, the perturbation method does not *per se* perform worse than the noise-stimulation methods. Yet, the prevention of overdriven PRCs is facilitated by the noise-stimulation methods compared to the perturbation method. Noise-stimulation data allows one to estimate the PRC based on the wSTA as well as the STEP method, and different PRC amplitudes in both measures provide a clear indication for overdriven PRCs.

Overdriven PRC estimates are a common problem in experimental studies. Farries and Wilson (2012a, b) report that even relatively large stimuli lead to reliable PRC estimates. Their solution to the problem of overdriven PRCs is a removal of the data points close to the causality limit. Others have related the causality limit to a biased sampling of phase (Phoka et al. 2010) or phase advance data (Wang et al. 2013). The authors propose methods to estimate the total distributions from the available, partial observations in order to get more realistic PRC estimates. While these approaches may help to extract more information from overdriven PRCs than the traditional analysis, they do not address the alterations in phase response due to the excessive stimulus amplitude discussed here.

The PRC amplitude is rarely reported in the literature, as many studies normalize the PRC amplitude arbitrarily, e.g., to one. This practice removes important information about the PRC: Not only is the amplitude required for any quantitative description of neuronal dynamics, it also provides a most valuable tool in testing for the overdriven regime. We stress that the correct amplitude scaling is as easily extracted from PRC data as the PRC shape itself.

Preventing overdriven PRCs becomes particularly relevant when measuring neurons with relatively high levels of intrinsic noise, such as cortical or hippocampal neurons, compared to neurons with stable repetitive firing. High levels of noise are also common when PRCs are estimated not for individual cells, but for whole brain areas. Recent studies indicated that measurements of PRCs for oscillating brain areas face similar challenges as measurements of neuronal PRCs. Significant phase jitter was for example reported in gamma oscillations (Nicholson et al. 2018), and the PRC depends on the stimulation amplitude, both in experimental recordings as well as Wilson-Cowan type models (Akam et al. 2012): PRCs measured for a hippocampal region are biphasic for weak stimulation, whereas strong stimulation leads – independent of the stimulation phase – to a stereotypical response, similar to the here reported instantaneous induction of the next spike in the overdriven regime (Akam et al. 2012). We conclude that the results gained in our study for neuronal oscillators can generalize to other types of phase oscillators. In cases with high levels of uncontrolled noise, attempted PRC measurements often suffer from exaggerated stimulus amplitudes in order to counter the intrinsic noise. In contrast, when measured with the appropriate stimulus amplitude, PRCs enrich our set of "diagnostic" tools to quantify neuronal dynamics.

Acknowledgements The study was funded by the German Federal Ministry of Education and Research (Grant No. 01GQ1403) and the German Research Foundation (GRK 1589). We thank Paul Pfeiffer for valuable feedback on the manuscript.

Compliance with Ethical Standards

Conflict of interests The authors declare that they have no conflict of interest.

Appendix: Conductance-based neuron models

Conductance-based neuron models were based on established models from the literature. The Hopf model was first described by Morris and Lecar; we use the version from Ermentrout and Terman (2010), p. 50-51. The SNIC and HOM models are versions of the Wang-Buzsaki model

(Wang and Buzsáki 1996). The membrane voltage v of the models follows the dynamics

$$\frac{\mathrm{d}v}{\mathrm{d}t} = (I_{\mathrm{in}} + g_{\mathrm{L}}(E_{\mathrm{L}} - v) + I_{\mathrm{gates}})/C_{\mathrm{m}}.$$

The input current is the sum of a DC current, a time-dependent stimulus and an intrinsic noise ξ, $I_{\mathrm{in}} = I_{\mathrm{DC}} + s(t) + \sigma\xi$. For simulations without intrinsic noise, $\sigma = 0$. The model parameters are summarized in Table 1.

Gating for the Hopf model:

For the Hopf model,

$$I_{\mathrm{gates}}(v, n) = g_{\mathrm{Na}} m_\infty(v)(E_{\mathrm{Na}} - v) + g_{\mathrm{K}} n(E_{\mathrm{K}} - v).$$

The kinetics of the ion channel gating n are given by

$$\frac{\mathrm{d}n}{\mathrm{d}t} = \phi \frac{n_\infty(v) - n}{\tau_n(v)},$$

with $\tau_n(v) = 1\mathrm{ms}/\cosh\left((v/\mathrm{mV} - 2)/60\right)$. The ion channel activation curves are given as

$$m_\infty(v) = 0.5(1 + \tanh((v/\mathrm{mV} - (-1.2))/18)),$$
$$n_\infty(v) = 0.5(1 + \tanh((v/\mathrm{mV} - 2)/30)).$$

Gating for the SNIC and HOM models:

For the SNIC model,

$$I_{\mathrm{gates}}(v, n, h) = g_{\mathrm{Na}} m_\infty(v)^3 h(E_{\mathrm{Na}} - v) + g_{\mathrm{K}} n^4(E_{\mathrm{K}} - v).$$

The kinetics of the ion channel gating are given by

$$\frac{\mathrm{d}h}{\mathrm{d}t} = \phi(\alpha_{\mathrm{h}}(v)(1 - h) - \beta_{\mathrm{h}}(v)h),$$
$$\frac{\mathrm{d}n}{\mathrm{d}t} = \phi(\alpha_{\mathrm{n}}(v)(1 - n) - \beta_{\mathrm{n}}(v)n),$$

Table 1 Parameters of the Hopf model and the SNIC model

Parameter	Hopf	SNIC
C_{m}	$20\mu\mathrm{F/cm}^2$	$1\mu\mathrm{F/cm}^2$
E_{L}	$-60\mathrm{mV}$	$-65\mathrm{mV}$
E_{Na}	$120\mathrm{mV}$	$55\mathrm{mV}$
E_{K}	$-84\mathrm{mV}$	$-90\mathrm{mV}$
g_{L}	$2\mathrm{mS/cm}^2$	$0.1\mathrm{mS/cm}^2$
g_{Na}	$4.4\mathrm{mS/cm}^2$	$35\mathrm{mS/cm}^2$
g_{K}	$8\mathrm{mS/cm}^2$	$9\mathrm{mS/cm}^2$
I_{DC}	$90.76\mu\mathrm{A/cm}^2$	$0.212\mu\mathrm{A/cm}^2$
ϕ	0.04	1

The HOM model is equivalent to the SNIC model, but with $\phi = 1.5$ and $I_{\mathrm{DC}} = 0.166\mu\mathrm{A/cm}^2$

Table 2 Stimulus amplitudes for different models and PRC estimation methods

Model	Stimulus strength α (perturbation method)
Hopf	$[500, 1443, 4163, 12011, 34657, 100000]\mu\mathrm{A/cm}^2$
SNIC	$[10, 25, 63, 158, 398, 1000]\mu\mathrm{A/cm}^2$
HOM	$[5, 11, 26, 58, 132, 300]\mu\mathrm{A/cm}^2$
Model	Stimulus strength γ (noise-stimulation method)
Hopf	$[1, 2.5, 6.3, 15.8, 39.8, 100]\mu\mathrm{A/cm}^2$
SNIC	$[0.03, 0.08, 0.19, 0.48, 1.19, 3]\mu\mathrm{A/cm}^2$
HOM	$[0.10, 0.25, 0.63, 1.58, 3.98, 10]\mu\mathrm{A/cm}^2$

with

$$\alpha_{\mathrm{h}}(v) = 0.07\exp(-\frac{v/\mathrm{mV} + 58}{20})/\mathrm{ms},$$
$$\beta_{\mathrm{h}}(v) = \frac{1}{1 + \exp(-0.1v/\mathrm{mV} - 2.8)}/\mathrm{ms},$$
$$\alpha_{\mathrm{n}}(v) = \frac{0.01v/\mathrm{mV} + 0.34}{1 - \exp(-0.1v/\mathrm{mV} - 3.4)}/\mathrm{ms},$$
$$\beta_{\mathrm{n}}(v) = 0.125\exp(-\frac{v/\mathrm{mV} + 44}{80})/\mathrm{ms},$$

The ion channel activation curve for the gating variable m is given as

$$m_\infty(v) = \frac{\alpha_{\mathrm{m}}(v)}{\alpha_{\mathrm{m}}(v) + 4\exp(-\frac{v/\mathrm{mV}+60}{18})},$$
$$\alpha_{\mathrm{m}}(v) = \frac{0.1v/\mathrm{mV} + 3.5}{1 - \exp(-0.1v/\mathrm{mV} - 3.5)}.$$

The HOM model is equivalent to the SNIC model, but with $\phi = 1.5$ and $I_{\mathrm{in}} = 0.166\mu\mathrm{A/cm}^2$, for more details see Hesse et al. (2017).

Conductance-based neuron models were simulated numerically with the simulation environment *brian2* (Stimberg et al. 2014). To record 500 perturbed spikes, the recording duration is 50 seconds for the noise-stimulation methods, and 100 seconds for the perturbation method, where only every second spike is perturbed. We observed that the interspike interval depends on the time resolution dt of the simulation. We have chosen $dt = 0.001\mathrm{ms}$ for all models, to ensure that a three times smaller time step changed the deterministic interspike interval by less than 5%.

To investigate the tolerance of PRC measurements towards an unknown noise source, PRCs were in a second step measured for neuron models that included intrinsic noise, implemented as an additive zero-mean white-noise current (the *brian2*-implemented variable `xi`). The noise levels chosen in this study correspond to relatively strong intrinsic noise, with a phase noise of $\tilde{\sigma} = 2\sqrt{\mathrm{ms}}$ or $\tilde{\sigma} = 3\sqrt{\mathrm{ms}}$ standard deviation (Fig. 4). The next section

shows how to translate the phase noise into the standard deviation of the *brian2*-implemented noise variable `xi`. The chosen phase noise results in a CV of around 0.2 and 0.3, respectively, which is within a biologically realistic range.

As a side-note, while the stimulus amplitude appropriate for PRC estimation is larger for perturbations than for a noise stimulus, the latter induce more spike jitter (larger CVs) compared to the perturbations. It seems that as the perturbation is temporally precise, even small spike deviations are sufficient to estimate PRCs, while the continuous input delivered by the noise stimulus requires larger deviations to estimate the PRC, probably because every spike informs about the full phase range, instead of just one particular phase.

Adaptation of intrinsic noise levels for brian2 models

Comparable levels of spike jitter between models can be ensured by balancing the effective phase noise. Let $\eta(t)$ be a zero-mean white noise current with standard deviation 1. As intrinsic noise current of the neuron model, we chose $\sigma\eta(t)$ with standard deviation σ. The phase Eq. (1) is $\dot{\varphi}(t) = 1 + Zs(t)$ with current input $s(t)$ and PRC Z. With the intrinsic noise as input, $s(t) = \sigma\eta(t)$, and under the assumption that the intrinsic noise is weak, and thus influences φ much less than the deterministic dynamics, one can replace the temporally precise filtering of the noise by its averaged effect in one interspike interval (Schleimer and Stemmler 2009). We get $\dot{\varphi}(t) = 1+\tilde{\sigma}\eta(t)$, with the variance of the white noise as $\tilde{\sigma}^2 = \sigma^2 \int_0^1 Z^2(\varphi)\mathrm{d}\varphi$.

Setting the phase noise $\tilde{\sigma}$ to the same value in all models, we find the appropriate current noise strength as $\sigma = \tilde{\sigma}\frac{C_\mathrm{m}}{T}\left[\int_0^1 Z^2(\varphi)\mathrm{d}\varphi\right]^{-0.5}$, where C_m is the membrane capacitance of the model. For the simulations, we evaluate this formula with the theoretical iPRCs gained from backwards integration of the adjoint equation as Z, see Section 2.3.

Error estimation by bootstrapping

In order to evaluate the quality of the PRC, we use a bootstrap approach to estimate errors for the phase response curves. Two different kinds of phase-dependent errors are considered, the baseline error which results from PRC estimates on shuffled data, and the error on the PRC estimate.

In order to provide an error for the PRC, we repetitively estimate PRCs using only a restricted amount of spikes. We estimated PRCs in 100 repetitions from a set about 250 spikes, randomly chosen from the total set of about 500 perturbed spikes. The standard deviation of the 100 PRC estimates was used as PRC error.

In order to provide a baseline for the PRC estimate – above which a significant PRC should rise – we measure PRCs for random combinations of noise snippets and spike advances. We measure the PRC in 100 repetitions for a random permutation of the numbering i of spike deviations $\{\Delta\varphi_i\}$, and calculate the standard deviation for the resulting 100 estimates. The mean of these estimates results in a PRC close to zero, such that the resulting standard deviation corresponds to the range within which a zero, i.e., non-significant PRC estimate is to be expected. This error around zero provides a lower bound to PRCs that are significantly different from zero.

Amplitude scaling for estimated phase-response curves

The appropriate unit for most experimentally derived PRCs is Hz cm$^2/\mu$A, which naturally arises for PRCs that measure the phase advance in response to a current per surface area, such as a noise stimulus or perturbation in μA/cm^2. For this study, however, we aim at comparing experimentally measured PRCs with theoretical iPRCs. The theoretical iPRCs gained from backwards integration of the adjoint equation have a unit of 1/mV, as they quantify the phase advance in response to a voltage perturbation in units of mV. For comparison, we transform the estimated PRCs into the units of the theoretical iPRCs by multiplying the current PRC by the membrane capacitance, $Z_{\Delta v} = Z_{\Delta I}\ C_\mathrm{m}$

References

Achuthan, S., Butera, R.J., Canavier, C.C. (2011). Synaptic and intrinsic determinants of the phase resetting curve for weak coupling. *Journal of Computational Neuroscience*, *30*(2), 373–390.

Akam, T., Oren, I., Mantoan, L., Ferenczi, E., Kullmann, D.M. (2012). Oscillatory dynamics in the hippocampus support dentate gyrus-CA3 coupling. *Nature Neuroscience*, *15*(5), 763–768.

Blankenburg, S., Wu, W., Lindner, B., Schreiber, S. (2015). Information filtering in resonant neurons. *Journal of Computational Neuroscience*, *39*(3), 349–370.

Brown, E., Moehlis, J., Holmes, P. (2004). On the phase reduction and response dynamics of neural oscillator populations. *Neural Computation*, *16*(4), 673–715.

Diba, K., Lester, H.A., Koch, C. (2004). Intrinsic noise in cultured hippocampal neurons: experiment and modeling. *Journal of Neuroscience*, *24*(43), 9723–9733.

Ermentrout, G.B., Galán, R.F., Urban, N.N. (2008). Reliability, synchrony and noise. *Trends in Neurosciences*, *31*(8), 428–434.

Ermentrout, G.B., & Kopell, N. (1991). Multiple pulse interactions and averaging in systems of coupled neural oscillators. *Journal of Mathematical Biology*, *29*(3), 195–217.

Ermentrout, B. (1996). Type I membranes, phase resetting curves, and synchrony. *Neural Computation*, *8*(5), 979–1001.

Ermentrout, G.B., & Terman, D.H. (2010). *Mathematical foundations of neuroscience*. Berlin: Springer Science & Business Media.

Farries, M.A., & Wilson, C.J. (2012a). Biophysical basis of the phase response curve of subthalamic neurons with generalization to other cell types. *Journal of Neurophysiology*, *108*(7), 1838–1855.

Farries, M.A., & Wilson, C.J. (2012b). Phase response curves of subthalamic neurons measured with synaptic input and current injection. *Journal of Neurophysiology*, *108*(7), 1822–1837.

Fellous, J.M., Houweling, A.R., Modi, R.H., Rao, R., Tiesinga, P., Sejnowski, T.J. (2001). Frequency dependence of spike timing reliability in cortical pyramidal cells and interneurons. *Journal of Neurophysiology*, *85*(4), 1782–1787.

Galán, R.F., Ermentrout, G.B., Urban, N.N. (2005). Efficient estimation of phase-resetting curves in real neurons and its significance for neural-network modeling. *Physical Review Letters*, *94*(15), 158101.

Goldberg, J.A., Deister, C.A., Wilson, C.J. (2007). Response properties and synchronization of rhythmically firing dendritic neurons. *Journal of Neurophysiology*, *97*(1), 208–219.

Govaerts, W., & Sautois, B. (2006). Computation of the phase response curve: a direct numerical approach. *Neural Computation*, *18*(4), 817–847.

Guevara, M.R., Glass, L., Shrier, A. (1981). Phase locking, period-doubling bifurcations, and irregular dynamics in periodically stimulated cardiac cells. *Science*, *214*(4527), 1350–1353.

Gutkin, B.S., Ermentrout, G.B., Reyes, A.D. (2005). Phase-response curves give the responses of neurons to transient inputs. *Journal of Neurophysiology*, *94*(2), 1623–1635.

Hansel, D., Mato, G., Meunier, C. (1995). Synchrony in excitatory neural networks. *Neural Computation*, *7*(2), 307–337.

Hesse, J., Schleimer, J.H., Schreiber, S. (2017). Qualitative changes in phase-response curve and synchronization at the saddle-node loop bifurcation. *Physical Review E*, *95*(5), 052203–25.

Hodgkin, A.L., & Huxley, A.F. (1952). A quantitative description of membrane current and its application to conduction and excitation in nerve. *The Journal of Physiology*, *117*(4), 500–544.

Izhikevich, E.M. (2000). Neural excitability, spiking and bursting. *International Journal of Bifurcation and Chaos*, *10*(6), 1171–1266.

Izhikevich, E.M. (2007). *Dynamical systems in neuroscience*. Cambridge: MIT Press.

Kuramoto, Y. (1984). *Chemical oscillations, waves and turbulence*. Berlin: Springer Science & Business Media.

Lazar, A.A. (2007). Information representation with an ensemble of Hodgkin-Huxley neurons. *Neurocomputing*, *70*(10–12), 1764–1771.

Mainen, Z.F., & Sejnowski, T.J. (1995). Reliability of spike timing in neocortical neurons. *Science*, *268*(5216), 1503–1506.

Manwani, A., & Koch, C. (1999). Detecting and estimating signals in noisy cable structures, ii: information theoretical analysis. *Neural Computation*, *11*(8), 1831–1873.

Minors, D.S., Waterhouse, J.M., Wirz-Justice, A. (1991). A human phase-response curve to light. *Neuroscience Letters*, *133*(1), 36–40.

Netoff, T.I., Acker, C.D., Bettencourt, J.C., White, J.A. (2005). Beyond two-cell networks: experimental measurement of neuronal responses to multiple synaptic inputs. *Journal of Computational Neuroscience*, *18*(3), 287–295.

Netoff, T.I., Banks, M.I., Dorval, A.D., Acker, C.D., Haas, J.S., Kopell, N., White, J.A. (2005). Synchronization in hybrid neuronal networks of the hippocampal formation. *Journal of Neurophysiology*, *93*(3), 1197–1208.

Netoff, T.I., Schwemmer, M.A., Lewis, T.J. (2011). Experimentally estimating phase response curves of neurons: theoretical and practical issues. In Schultheiss, N.W., Prinz, A.A., Butera, R.J. (Eds.) *Phase Response Curves in Neuroscience: theory, Experiment, and Analysis*, (Vol. 5 pp. 95–129). Berlin: Springer Science & Business Media.

Nicholson, E., Kuzmin, D.A., Leite, M., Akam, T.E., Kullmann, D.M. (2018). Analogue closed-loop optogenetic modulation of hippocampal pyramidal cells dissociates gamma frequency and amplitude. *eLife*, *7*, e38346.

Ota, K., Nomura, M., Aoyagi, T. (2009). Weighted spike-triggered average of a fluctuating stimulus yielding the phase response curve. *Physical Review Letters*, *103*(2), 024101.

Phoka, E., Cuntz, H., Roth, A., Häusser, M. (2010). A new approach for determining phase response curves reveals that purkinje cells can act as perfect integrators. *PLoS Comput Biol*, *6*(4), e1000768.

Razali, N., & Wah, Y.B. (2011). Power comparisons of Shapiro-Wilk, Kolmogorov-Smirnov, Lilliefors and Anderson-Darling tests. *Journal of Statistical Modeling and Analytics.*, *2*(1), 21–33.

Reyes, A.D., & Fetz, E.E. (1993a). Effects of transient depolarizing potentials on the firing rate of cat neocortical neurons. *Journal of Neurophysiology*, *69*(5), 1673–1683.

Reyes, A.D., & Fetz, E.E. (1993b). Two modes of interspike interval shortening by brief transient depolarizations in cat neocortical neurons. *Journal of Neurophysiology*, *69*(5), 1661–1672.

Rinzel, J., & Ermentrout, G.B. (1989). *Analysis of neural excitability and oscillations*, (pp. 135–169). Cambridge: MIT Press.

Schleimer, J.H., & Stemmler, M. (2009). Coding of information in limit cycle oscillators. *Physical Review Letters*, *103*(24), 248105.

Schleimer, J.H., & Schreiber, S. (2018). Phase-response curves of ion channel gating kinetics. *Mathematical Methods in the Applied Sciences*, *41*(18), 8844–8858.

Schreiber, S., Samengo, I., Herz, A.V.M. (2009). Two distinct mechanisms shape the reliability of neural responses. *Journal of Neurophysiology*, *101*(5), 2239–2251.

Schultheiss, N.W., Prinz, A.A., Butera, R.J. (2011). *Phase response curves in neuroscience: theory, experiment and analysis*. Berlin: Springer Science & Business Media.

Smeal, R.M., Ermentrout, G.B., White, J.A. (2010). Phase-response curves and synchronized neural networks. *Philosophical Transactions of the Royal Society B: Biological Sciences*, *365*(1551), 2407–2422.

Stiefel, K.M., & Ermentrout, G.B. (2016). Neurons as oscillators. *Journal of Neurophysiology*, *116*(6), 2950–2960.

Stimberg, M., Goodman, D.F.M., Benichoux, V., Brette, R. (2014). Equation-oriented specification of neural models for simulations. *Frontiers in Neuroinformatics*, *8*, 6.

Teramae, Jn., & Fukai, T. (2008). Temporal precision of spike response to fluctuating input in pulse-coupled networks of oscillating neurons. *Physical Review Letters*, *101*(24), 248105.

Torben-Nielsen, B., Uusisaari, M., Stiefel, K.M. (2010a). A Comparison of methods to determine neuronal phase-response curves. *Frontiers in Neuroinformatics* 4.

Torben-Nielsen, B., Uusisaari, M., Stiefel, K.M. (2010b). A novel method for determining the phase-response curves of neurons based on minimizing spike-time prediction error. arXiv:10010446 [q-bio].

Tsubo, Y., Takada, M., Reyes, A.D., Fukai, T. (2007). Layer and frequency dependencies of phase response properties of pyramidal neurons in rat motor cortex. *European Journal of Neuroscience*, *25*(11), 3429–3441.

Van Vreeswijk, C., Abbott, L.F., Ermentrout, G.B. (1994). When inhibition not excitation synchronizes neural firing. *Journal of Computational Neuroscience*, *1*(4), 313–321.

Wang, X.J., & Buzsáki, G. (1996). Gamma oscillation by synaptic inhibition in a hippocampal interneuronal network model. *The Journal of Neuroscience*, *16*(20), 6402–6413.

Wang, S., Musharoff, M.M., Canavier, C.C., Gasparini, S. (2013). Hippocampal CA1 pyramidal neurons exhibit type 1 phase-response curves and type 1 excitability. *Journal of Neurophysiology*, *109*(11), 2757–2766.

White, J.A., Klink, R., Alonso, A., Kay, A.R. (1998). Noise from voltage-gated ion channels may influence neuronal dynamics in the entorhinal cortex. *Journal of Neurophysiology*, *80*(1), 262–269.